

Multistable Kuramoto splay states in a crystal of mode-locked laser pulses

T. G. Seidel,^{1,2} A. Bartolo,^{3,4} A. Garnache,³ M. Giudici,⁴ M. Marconi,⁴ S. V. Gurevich,^{1,2} and J. Javaloyes²

¹*Institute for Theoretical Physics, University of Münster, Wilhelm-Klemm-Str.9 48149 Münster, Germany*

²*Departament de Física and IAC³, Universitat de les Illes Balears, C/ Valldemossa km 7.5, 07122 Mallorca, Spain*

³*Institut d'Electronique et des Systèmes, CNRS UMR5214, 34000 Montpellier, France*

⁴*Université Côte d'Azur, CNRS, Institut de Physique de Nice, 06200 Nice, France*

We demonstrate the existence of a multiplicity of co-existing frequency combs in a harmonically mode-locked laser that we link to the splay phases of the Kuramoto model with short range interactions. These splay states are multistable and the laser may wander between them under the influence of stochastic forces. Consequently, the many pulses circulating in the cavity are not necessarily coherent with each other. We show that this partially disordered state for the phase of the optical field features regular train of pulses in the field intensity, a state that we term an incoherent crystal of optical pulses. We provide evidence that the notion of coherence should be interpreted by comparing the duration of the measurement time with the Kramers' escape time of each splay state. Our results are confirmed experimentally by studying a passively mode-locked vertical external-cavity surface-emitting laser.

The realization of mode-locking (ML) has been a milestone of laser physics as it allowed to generate the ultrashort pulses that are of paramount importance in many fields including medicine, metrology and communications [1]. The term ML stems from the synchronous oscillation, i.e. the phase locking of many electromagnetic modes in a cavity. The emergence of such macroscopic coherent states, either spontaneously or under periodic forcing, can be seen as the critical point of an out-of-equilibrium ferromagnetic phase transition [2–4] establishing a link between modal self-organization and frequency combs in active cavities [5, 6]. The applications of ML encompass radio-over-fibre [7], two-photon absorption microscopy [8] or dual comb spectroscopy [9]. The fundamental importance of mode-locked lasers is demonstrated by their link with dissipative solitons [10], their generalization to spatio-temporal systems [11–14] or their capability as Ising Photonic Machines to solve NP hard problems and perform Boltzmann sampling [15–17].

Soon after their inception, it was demonstrated that a pulsating laser can also operate in the so-called harmonic mode-locked (HML) regime, a state in which the laser cavity supports a train of $N \in \mathbb{N}$ equidistant pulses (denoted here as HML_N) [18], see Fig. 1(a). This effectively reduces the pulse train period to τ/N with τ the cavity round-trip, while circumventing the difficulties inherent in using shorter cavities. These regular pulse arrangements can be identified spectrally since the repetition rate multiplication corresponds to an equivalent N -fold increase in the distance between spectral lines, that becomes a multiple of the fundamental free spectral range (FSR), i.e. N/τ . Such states have been widely observed in mode-locked fiber lasers [19–21] but also in optical systems with broken phase symmetry such as optically injected Kerr micro-cavities [22, 23]. In the latter, regular pulse trains, also termed “soliton crystals”, are phase locked to an external reference beam which leads to a unique, well-defined, frequency comb. The phase invariance of the electromagnetic field in a mode-locked laser radically modifies the picture as it allows each pulse to

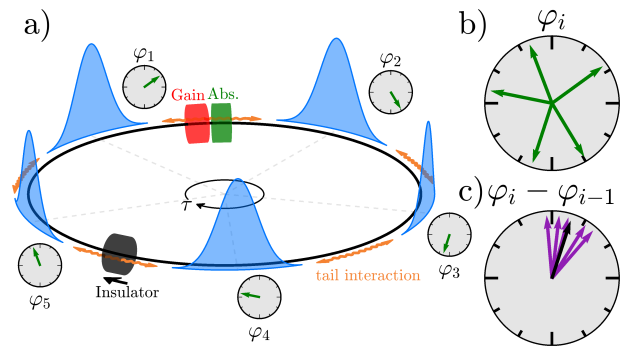


FIG. 1. a) Schematic of a unidirectional ring cavity mode-locked by a saturable absorber and operated in the HML_5 regime. Each pulse possesses a phase φ_i , as indicated by the small clocks. The phases and their differences are shown in b) and c) while the black arrow in c) denotes to value of the order parameter b representing the average coherence.

possess a *different* phase φ_i with $i \in [1, N]$, see Fig. 1(b).

In this letter, we ask the seemingly naive question: are the N pulses circulating in a HML cavity necessarily coherent with each other? What are their phase relations (if any) and, could an incoherent mode-locked crystal of pulses simply exist?

For the purpose of illustration, we shall consider a passively mode-locked unidirectional ring laser as depicted in Fig. 1 and in which a saturable absorber promote pulsed emission. The multi-pulse HML dynamics can be studied using the well established Haus master equation [24, 25] that links the evolution of the electric field (E), the gain (g) and absorber population (q),

$$\partial_\theta E = \left(\frac{1}{2\gamma_f^2} \partial_z^2 + \frac{1 - i\alpha_g}{2} g - \frac{1 - i\alpha_q}{2} q - k \right) E + \sigma \xi, \quad (1)$$

$$\partial_z g = \Gamma (g_0 - g) - g |E|^2, \quad \partial_z q = q_0 - q - sq |E|^2. \quad (2)$$

Here, z and θ denote the fast and slow time scales which describe the evolution within one round-trip and from

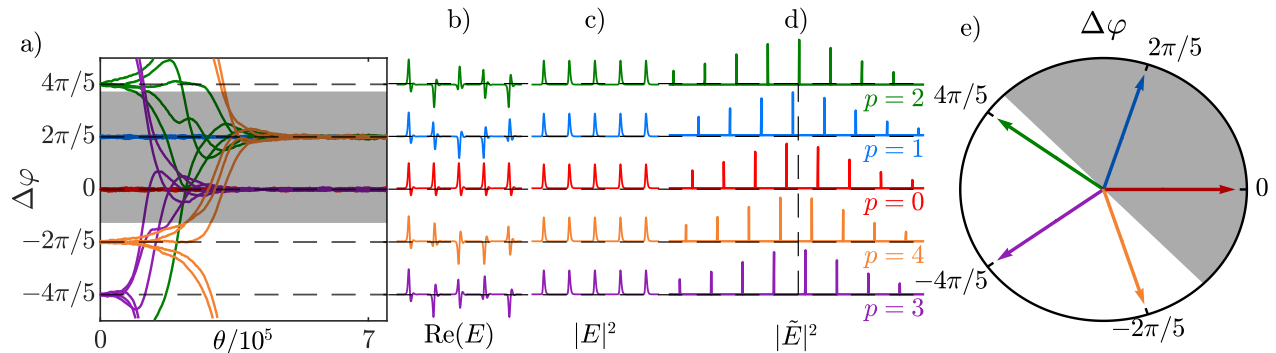


FIG. 2. a) Time evolution of various splay states associated to the HML₅ solutions obtained from solving Eqs. (1-2) numerically. The initial phase differences are given by $\Delta\varphi_p = \frac{2\pi}{N}p$, and are shown in panels b) and c) where one can see that the intensity profiles are identical while the real parts of the electric fields differ. d) Frequency spectrum of the initial conditions. For each phase difference the corresponding comb is shifted by $\frac{p}{\tau}$. e) Phase plane visualization of the initial conditions used in a)-d). The shaded gray areas in panels a) and e) correspond to the region of stability which is of size π . The trajectories in a) converge to steady states within the region of stability. Parameters are $(\gamma_f, k, \alpha, \beta, \tau, g_0, \Gamma, q_0, s, \sigma) = (40, 0.8, 1.5, 0.5, 12.5, 4g_{th}, 0.08, 0.3, 10, 10^{-5})$ and corresponds to a 5 GHz mode-locked laser emitting 14 ps pulses (FWHM).

one round-trip to the next one, respectively. Further, the gain bandwidth is γ_f , the cavity losses are k and $\alpha_{g,q}$ correspond either to the linewidth enhancement factors for semiconductor material or the transition line detuning in atomic gain media. Time is normalized to the absorber recovery time of 80 ps and the gain recovery rate is denoted as Γ , while the ratio of the saturation energy of the gain and the absorber media is s . For simplicity, we model the spontaneous emission fluctuations and the mechanical vibrations in the cavity potentially impacting coherence with additive white Gaussian noise of the amplitude σ in Eq. (1). The equations (1,2) were complemented with the dynamical boundary conditions detailed in [25]. However, we note that identical conclusions were obtained using periodic boundaries or by using instead the first principle time-delayed model of [26]. The coherence of a regular HML state can be measured by the order parameter $b = \frac{1}{N} \sum_j \exp[i(\varphi_j - \varphi_{j-1})]$, which is equivalent to the first order field correlation $g^{(1)}(\frac{\tau}{N})$ for a train of equidistant pulses that are identical up to a phase, see Supplementary Material (SM). Perfect order corresponds to $|\langle b \rangle| = 1$, see Fig. 1(c), whereas full disorder yields $|\langle b \rangle| = 0$. The bracket denotes a temporal average over many cavity round-trips. In order to derive in which configurations the pulses can exist in an HML regime, it is sufficient to consider the ring boundary conditions in Fig. 1(a). A steady state can only exist if the phase difference $\Delta\varphi$ between neighboring pulses is constant. This condition can only be fulfilled if $N\Delta\varphi = 2\pi p$ with $p \in [0, N-1]$. As such, the steady states are characterized by the integer index p or equivalently a phase difference $\Delta\varphi_p = \frac{2\pi}{N}p$, which is the definition of a *splay*

state [27]. We note that a phase shift $\Delta\varphi_p$ between pulses separated by a distance $\Delta z = \tau/N$ corresponds to an offset of the carrier frequency $\nu_p = \Delta\varphi_p / (2\pi\Delta z) = p/\tau$. Consequently, these N splay states correspond to frequency combs that are shifted of p times the fundamental FSR of the cavity, see Fig. 2(b-d).

Pulses interact via the active material dynamics. When a pulse crosses over the amplifier, it depletes its available gain, that only partially recovers before the arrival of the next pulse. This leads to a repulsion between pulses [28, 29]. For short cavities where $\Gamma\tau < 1$, the positions of the pulses are tightly bound, as in a crystal, to $z_j = j\tau/N$. In addition, pulses also possess phase sensitive interactions with their neighbors via the overlap of their decaying tails, see Fig. 1(a). Assuming exponential tails, this coherent effect scales as $\exp(-\tau_s/\tau_p) \ll 1$ with τ_s the separation between pulses and τ_p the pulse width. Consequently, the phase of each pulse evolves in relation with that of its nearest neighbors over a time scale much larger than the round-trip. We note that previous works demonstrated coherence in a HML laser with a ratio $\tau_s/\tau_p \simeq 23$ [20] indicating that this nearest neighbor interaction is extremely weak. While ratios up to $\tau_s/\tau_p \simeq 50$ where reported in [30], the relevance of this weak interaction must be compared with the amount of spontaneous emission and technical noise leading to decoherence.

Intuition about the phase evolution can be obtained by projecting the dynamics of the high-dimensional Haus Eqs. (1,2) onto a low-dimensional subspace that correspond to the slow evolution of the weakly coupled phase modes. This central manifold reduction reads

$$\partial_\theta \varphi_j = A_+ \sin(\varphi_{j-1} - \varphi_j + \psi_+) + A_- \sin(\varphi_{j+1} - \varphi_j + \psi_-) + \sigma \xi_j(t), \quad \varphi_0 = \varphi_N, \quad j \in [1, N]. \quad (3)$$

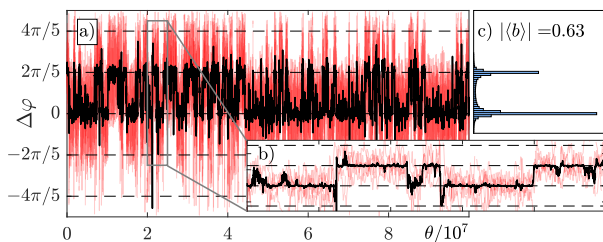


FIG. 3. a) Time evolution of phase differences of five pulses (light red) for the same parameters as in Fig. 2 obtained from a direct numerical simulation of Eqs. (1,2) with added noise of amplitude $\sigma = 4 \times 10^{-4}$. Other parameters are as in Fig. 1. The black line denotes the phase of the order parameter b . As the system is bistable for $N = 5$, the order parameter jumps between the two stable steady states $\Delta\varphi_{0,1} = 0, \frac{2\pi}{5}$. b) Zoomed view around a region with multiple jumps. c) Statistical distribution of the phases visited by arg b . The two peaks correspond to the two aforementioned steady states.

We denote (A_{\pm}, ψ_{\pm}) the amplitudes and phases of the coupling forces with the left and right neighboring pulses. The parameters ψ_{\pm} are inherited from the asymmetrical and possibly chirped nature of the pulses. For $\psi_{\pm} \neq 0$ the interactions are non-variational, i.e. Eq. (3) can not be derived from an interaction potential. In addition, since the pulses are *a priori* not symmetrical, $A_+ \neq A_-$ which renders their interactions non-reciprocal. This situates our work in the emerging field of non-conservative and non-reciprocal interactions [31, 32]. Finally, $\xi_j(t)$ is a Gaussian white noise whose amplitude σ corresponds to the projection of the original stochastic process in Eq. (1) over the phase dynamics. We note that Eq. (3) corresponds to the Kuramoto model with short range (nearest neighbor) interactions, which is also known as the dissipative XY model, see [33] and reference therein. A linear stability analysis of Eq. (3) reveals that a splay state is stable if $\alpha_0 < \Delta\varphi_p < \alpha_1$ with

$$\alpha_k = k\pi + \arctan\left(\frac{A_- \cos \psi_- + A_+ \cos \psi_+}{A_- \sin \psi_- - A_+ \sin \psi_+}\right). \quad (4)$$

We observe that the range of stability is always π and that the half-circle of stability is simply rotated as a function of (A_{\pm}, ψ_{\pm}) . The most important consequence of Eq. (4) is that the splay states that are solutions of Eq. (3) can be *multistable*. In fact, for $N \geq 5$, there must be at least two states that fall within the range of stability and 50% of states are stable in the thermodynamic limit $N \rightarrow \infty$. In order to test our predictions we performed numerical simulations of the original Haus master Eqs. (1,2), which we initialized with the five different splay states, see Fig. 2(a,b). We stress that all these solutions correspond to the same intensity profile as demonstrated in Fig. 2(c). The rotation of the field $\Delta\varphi_p$ from one pulse to the next creates a p/τ frequency-shifted comb, see Fig. 2(d). We observe that two initial conditions remain stable upon their time evolution as

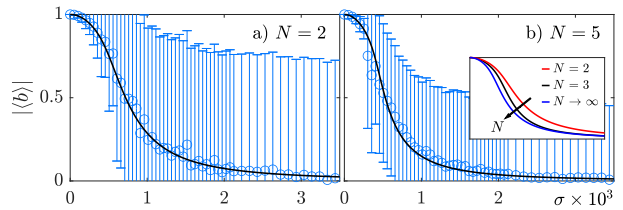


FIG. 4. The order parameter $|\langle b \rangle|$ as a function of noise for different numbers of pulses in the cavity (blue: Haus Eqs. (1,2), black: phase model in Eq. (3)). The cavity round-trip is increased according to the HML number as $\tau = N \times 2.5$. Same parameters as in Figs. 2 and Fig. 3. Inset in b): analytical result for the Hamiltonian phase model.

they lie within the stable region defined by Eq. (4) and marked by the gray areas in Fig. 2(a,e). The other three trajectories correspond to unstable states and converge to one of the two stable configurations, cf. Fig. 2(a). The parameters (A_{\pm}, ψ_{\pm}) in Eq. (3) were extracted from Eqs. (1,2) by using a perturbation analysis.

The prediction of multistability for $N \geq 5$ has a profound consequence on the measurement of the coherence as it must naturally be interpreted by comparing the Kramers' escape time of each splay state [34] and the duration of the measurement time. The latter typically occurs experimentally over a time scale of a second, which corresponds to billions of round-trips. We show in Fig. 3(a) the result of a long simulation of Eqs. (1,2) over 10^8 round-trips, i.e. ~ 0.4 s for $\tau = 4.4$ ns. Due to the presence of noise, the system is able to visit many times all the stable states. This can be seen best in Fig. 3(b) which provides a zoom around a small part of the original time trace. We note that visiting the unstable states is also possible for higher noise amplitudes and that the noise amplitude used here only give rise to a 5 % fluctuation of the pulse peak power (cf. Figs. 1,2 of the SM). We detail in Fig. 3(c) a histogram of the value of arg b . Due to the low noise value, the distribution is narrowly peaked around each stable splay state and the theoretical value of the order parameter should be $\langle b_p \rangle = \exp(i\Delta\varphi_p)$. Indeed, if the value of the coherence $|\langle b \rangle|$ is calculated over a time smaller than the average residence time, we found $|\langle b \rangle| \sim 0.95$. If instead the coherence is measured over the entire time trace, we obtain $|\langle b \rangle| = 0.63$ which is the result of the partial cancellation between $\langle b_0 \rangle$ and $\langle b_1 \rangle$.

Having demonstrated the good agreement between Eqs. (1,2) and Eq. (3) we used a combination of the two to perform an extended analysis as a function of N and the noise level. As the number of stable states grows with N bringing the splay states closer together and diminishing the potential barrier between them one can wonder how stable a single splay state can be if, e.g. $N = 350$ as discussed in [20]? Our results are summarized in Fig. 4. We notice that if the amplitude of the noise is too low, the system will not be able to jump from one steady state to the other leading to a coherence close to unity. On the other hand, if it is too high in comparison with the force

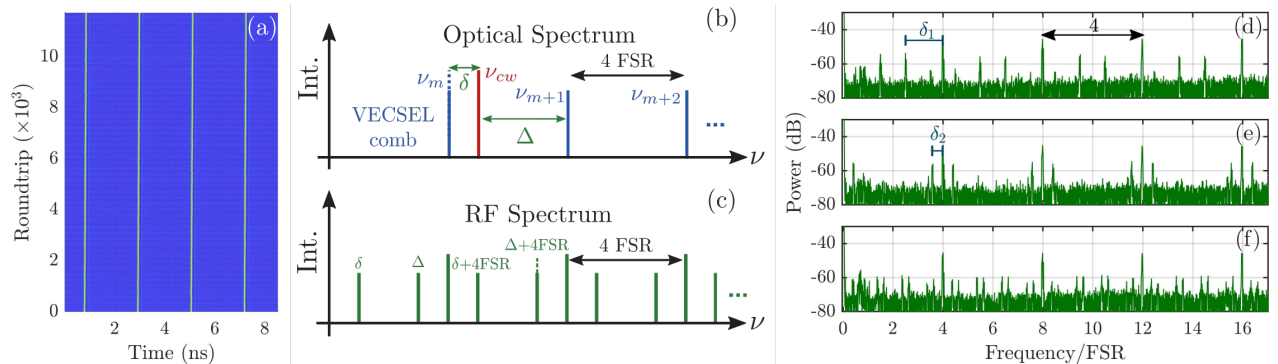


FIG. 5. a) Space-time diagram of the laser output showing four equidistant pulses. Central column. b) Spectral illustration of the heterodyne beating between a splay state of four pulses and a CW laser. c) Illustration of the resulting RF spectrum obtained from the heterodyne beating in b). Right column: RF spectra of the heterodyne beating signal. d,e) Two examples of coherent splay states with a spectral shift of one FSR. f) Incoherent splay state characterized by the average spectral emission composed by spectral lines separated by one FSR.

between pulses, i.e. $\sigma \gg A_{\pm}$, coherence is entirely lost as $|\langle b \rangle| \rightarrow 0$. We note that in this case, the system continues to generate a very regular intensity pulse train and it can therefore be interpreted as an *incoherent crystal*. Finally, we confirm that the coherence decays faster for larger values of N as it is averaged over a larger number of states. The numerical curves in Fig. 4 (in blue) were fitted with the analytical formula for the coherence (in black) of the Hamiltonian XY model [35] that shares the same steady states as Eq. (3) (cf. SM for details).

To confirm our theoretical predictions, we implemented an experimental setup consisting of a vertical external-cavity surface-emitting laser mode-locked using a semiconductor saturable absorber mirror as in [36]. The laser cavity (see SM) has a round-trip time $\tau = 8.5$ ns. For this value of τ , the optical pulses can be addressed on and off independently [37] although they become equidistant rapidly due to the repulsive incoherent forces discussed above. This leads to the multistability of the HML states with $N \in [0, 8]$. The laser output is sent to a heterodyne measurement setup that analyzes the spectral features of the pulse train. By beating the laser output with a stable CW laser source, we convert a portion of the optical spectrum into the RF domain (see SM). We analyze the coherence of a pulse train consisting of 4 equidistant pulses. Figure 5(a) shows a spatio-temporal map of the laser intensity for the HML₄ solution, where the horizontal axis represents the round-trip time and the vertical axis is the number of round-trips, which highlights that the pulses are perfectly equispaced, have the same amplitude, and are stable over more than 10 000 round-trips. Figure 5(b,c) describes the principle of the heterodyne measurement. Panel (b) schematically illustrates the optical spectrum of a mode-locked laser that is emitting on a coherent splay state with $N = 4$. Due to the coherent interaction between the pulses, the spectrum is composed of equidistant lines every 4 FSR. The CW laser frequency is represented in red and the beating

frequencies are shown in green. The corresponding RF signal is shown in panel (c).

The jump from one coherent splay state $\Delta\varphi_p$ to another $\Delta\varphi_q$ should manifest in the optical spectrum by a $(p - q)$ -harmonic FSR shift while the interference pattern should keep the same visibility (see SM). The heterodyne optical spectra (cf. the right column of Fig. 5) reveal the various splay states explored by the system. Figure 5(d) shows a situation identical to the example depicted in panel (c), which indicates that the pulsed solution is a coherent splay state. In panel (e), the RF spectrum shows the same features as panel (d) but the lines in the optical spectrum are shifted with respect to the previous case. In accordance with the theory, the shift experienced by the optical lines corresponds to one FSR of the laser optical spectrum, as demonstrated in the Supplementary Material. Figure 5(f) reveals that the pulse train can also be incoherent, as predicted from the theoretical analysis. This incoherent state is characterized by phase jumps which are responsible for the emergence of multiple beating lines in the optical spectrum. Here, the maximum number of 8 lines (2 beat tones times 4 possible FSR jumps) is obtained, which indicates that within the acquisition time of the RF spectrum analyzer (20 ms), the phase differences between the pulses have explored all the four stable and unstable possible configurations (from 0 to $3\pi/4$), i.e. the modal separation is one FSR. This observation demonstrates that a pulse train can be stable in intensity, while the phase difference between consecutive pulses can vary in time.

In conclusion, we have demonstrated that the harmonic pulse trains emitted by a mode-locked semiconductor laser is equivalent to the splay-phase states of the Kuramoto model with short range interactions. The multistability between frequency combs was demonstrated experimentally and we could observe the coherence parameter $|b|$ jumping between high and vanishing values. This implies that the notion of coherence must be inter-

preted by comparing the duration of the measurement time with the Kramers' escape time of each splay state, which can be extremely long due to the small amplitude of noise and of the weak pulse interactions. We disclosed that this partially disordered state for the phase of the optical field features regular train of pulses in the field intensity, a state we termed an incoherent optical crystal. Next, we showed how the laser cavity can experience a continuous shift from coherence to incoherence as a function of the number of pulses as well as the ratio between stochastic forces and the tail overlap between pulses. The multistability induced by the splay phases can potentially be controlled and used as a degree of freedom for encoding information in mode-locked lasers. Finally, we stress that we used a minimal model only considering nearest neighbor coupling which was sufficient to show the transition from coherent to incoherent emission and explain

the experimental results. Additional couplings arising from time-delayed feedback, as in [37], or intra-cavity lenses reflection would induce further non-local coupling between pulses and lead to an even richer phenomenology, as observed in other fields [38–40].

ACKNOWLEDGMENTS

We acknowledge the financial support of the project KOGIT, Agence Nationale de la Recherche (No. ANR-22-CE92-0009) and Deutsche Forschungsgemeinschaft (DFG) via Grant No. 505936983. TGS and JJ acknowledge funding from the Studienstiftung des Deutschen Volkes and the Ministerio de Economía y Competitividad (PID2021-128910NB-100 AEI/FEDER UE, PGC2018-099637-B-100 AEI/FEDER UE), respectively.

-
- [1] H.A. Haus. Mode-locking of lasers. *IEEE J. Selected Topics Quantum Electron.*, 6(6):1173–1185, 2000.
- [2] A. Gordon and B. Fischer. Phase transition theory of many-mode ordering and pulse formation in lasers. *Physical Review Letters*, 89:103901–3, 2002.
- [3] R. Weill, A. Rosen, A. Gordon, O. Gat, and B. Fischer. Critical behavior of light in mode-locked lasers. *Physical Review Letters*, 95:013903, 2005.
- [4] L. Leuzzi, C. Conti, V. Folli, L. Angelani, and G. Ruocco. Phase diagram and complexity of mode-locked lasers: From order to disorder. *Phys. Rev. Lett.*, 102:083901, Feb 2009.
- [5] Johannes Hillbrand, Dominik Auth, Marco Piccardo, Nikola Opačak, Erich Gornik, Gottfried Strasser, Federico Capasso, Stefan Breuer, and Benedikt Schwarz. In-phase and anti-phase synchronization in a laser frequency comb. *Phys. Rev. Lett.*, 124:023901, Jan 2020.
- [6] L. Columbo, M. Piccardo, F. Prati, L. A. Lugiato, M. Brambilla, A. Gatti, C. Silvestri, M. Giovannini, N. Opačak, B. Schwarz, and F. Capasso. Unifying frequency combs in active and passive cavities: Temporal solitons in externally driven ring lasers. *Phys. Rev. Lett.*, 126:173903, Apr 2021.
- [7] D. Novak, Z. Ahmed, R.B. Waterhouse, and R.S. Tucker. Signal generation using pulsed semiconductor lasers for application in millimeter-wave wireless links. *Microwave Theory and Techniques, IEEE Transactions on*, 43(9):2257–2262, sep 1995.
- [8] Masaru Kuramoto, Nobuyoshi Kitajima, Hengchang Guo, Yuji Furushima, Masao Ikeda, and Hiroyuki Yokoyama. Two-photon fluorescence bioimaging with an all-semiconductor laser picosecond pulse source. *Opt. Lett.*, 32(18):2726–2728, Sep 2007.
- [9] S. M. Link, D. J. H. C. Maas, D. Waldburger, and U. Keller. Dual-comb spectroscopy of water vapor with a free-running semiconductor disk laser. *Science*, 2017.
- [10] P. Grelu and N. Akhmediev. Dissipative solitons for mode-locked lasers. *Nat Photon*, 6(2):84–92, 2012.
- [11] Aleksander K. Wójcik, Nanfang Yu, Laurent Diehl, Federico Capasso, and Alexey Belyanin. Self-synchronization of laser modes and multistability in quantum cascade lasers. *Phys. Rev. Lett.*, 106:133902, Apr 2011.
- [12] Logan G. Wright, Pavel Sidorenko, Hamed Pourbeyram, Zachary M. Ziegler, Andrei Isichenko, Boris A. Malomed, Curtis R. Menyuk, Demetrios N. Christodoulides, and Frank W. Wise. Mechanisms of spatiotemporal mode-locking. *Nature Physics*, 16(5):565–570, May 2020.
- [13] Yihang Ding, Xiaosheng Xiao, Kewei Liu, Shuzheng Fan, Xiaoguang Zhang, and Changxi Yang. Spatiotemporal mode-locking in lasers with large modal dispersion. *Phys. Rev. Lett.*, 126:093901, Mar 2021.
- [14] Logan G. Wright, William H. Renninger, Demetri N. Christodoulides, and Frank W. Wise. Nonlinear multimode photonics: nonlinear optics with many degrees of freedom. *Optica*, 9(7):824–841, Jul 2022.
- [15] Shuhei Tamate, Yoshihisa Yamamoto, Alireza Marandi, Peter McMahon, and Shoko Utsunomiya. Simulating the classical xy model with a laser network. *arxiv*, 2016.
- [16] Takahiro Inagaki, Kensuke Inaba, Ryan Hamerly, Kyo Inoue, Yoshihisa Yamamoto, and Hiroki Takesue. Large-scale ising spin network based on degenerate optical parametric oscillators. *Nature Photonics*, 10(6):415–419, Jun 2016.
- [17] Y Takeda, S Tamate, Y Yamamoto, H Takesue, T Inagaki, and S Utsunomiya. Boltzmann sampling for an xy model using a non-degenerate optical parametric oscillator network. *Quantum Science and Technology*, 3(1):014004, nov 2017.
- [18] M. Becker, D. Kuizenga, and A. Siegman. Harmonic mode locking of the nd:yag laser. *IEEE Journal of Quantum Electronics*, 8(8):687–693, 1972.
- [19] A. B. Grudinin and S. Gray. Passive harmonic mode locking in soliton fiber lasers. *J. Opt. Soc. Am. B*, 14(1):144–154, Jan 1997.
- [20] Adil Haboucha, Hervé Leblond, Mohamed Salhi, Andrey Komarov, and François Sanchez. Coherent soliton pattern formation in a fiber laser. *Opt. Lett.*, 33(5):524–526, Mar 2008.
- [21] Foued Amrani, Mohamed Salhi, Philippe Grelu, Hervé Leblond, and François Sanchez. Universal soliton pattern formations in passively mode-locked fiber lasers. *Opt. Lett.*, 36(9):1545–1547, May 2011.

- [22] Daniel C. Cole, Erin S. Lamb, Pascal Del’Haye, Scott A. Diddams, and Scott B. Papp. Soliton crystals in kerr resonators. *Nature Photonics*, 11(10):671–676, Oct 2017.
- [23] Maxim Karpov, Martin H. P. Pfeiffer, Hairun Guo, Wenle Weng, Junqiu Liu, and Tobias J. Kippenberg. Dynamics of soliton crystals in optical microresonators. *Nature Physics*, 15(10):1071–1077, Oct 2019.
- [24] H. A. Haus, M. Margalit, and C. X. Yu. Quantum noise of a mode-locked laser. *Journal of the Optical Society of America B*, 17:1240–1256, 2000.
- [25] Jan Hausen, Kathy Lüdige, Svetlana V. Gurevich, and Julien Javaloyes. How carrier memory enters the haus master equation of mode-locking. *Opt. Lett.*, 45(22):6210–6213, Nov 2020.
- [26] A. G. Vladimirov and D. Turaev. Model for passive mode locking in semiconductor lasers. *Phys. Rev. A*, 72:033808, Sep 2005.
- [27] Rico Berner, Serhiy Yanchuk, Yuri Maistrenko, and Eckehard Schöll. Generalized splay states in phase oscillator networks. *Chaos: An Interdisciplinary Journal of Nonlinear Science*, 31(7):073128, 07 2021.
- [28] J.N. Kutz, B.C. Collings, K. Bergman, and W.H. Knox. Stabilized pulse spacing in soliton lasers due to gain depletion and recovery. *Quantum Electronics, IEEE Journal of*, 34(9):1749–1757, Sep 1998.
- [29] J. Javaloyes, P. Camelin, M. Marconi, and M. Giudici. Dynamics of localized structures in systems with broken parity symmetry. *Phys. Rev. Lett.*, 116:133901, Mar 2016.
- [30] Philippe Grellu, Franck Belhache, François Gutty, and Jose M. Soto-Crespo. Relative phase locking of pulses in a passively mode-locked fiber laser. *J. Opt. Soc. Am. B*, 20(5):863–870, May 2003.
- [31] Michel Fruchart, Ryo Hanai, Peter B. Littlewood, and Vincenzo Vitelli. Non-reciprocal phase transitions. *Nature*, 592(7854):363–369, Apr 2021.
- [32] Sabine H. L. Klapp. Non-reciprocal interaction for living matter. *Nature Nanotechnology*, 18(1):8–9, Jan 2023.
- [33] Juan A. Acebrón, L. L. Bonilla, Conrad J. Pérez Vicente, Félix Ritort, and Renato Spigler. The kuramoto model: A simple paradigm for synchronization phenomena. *Rev. Mod. Phys.*, 77:137–185, Apr 2005.
- [34] C. W. Gardiner. *Handbook of stochastic methods. 2nd Ed.* Springer-Verlag, Berlin, 1995.
- [35] J M Kosterlitz and D J Thouless. Ordering, metastability and phase transitions in two-dimensional systems. *Journal of Physics C: Solid State Physics*, 6(7):1181, apr 1973.
- [36] A. Bartolo, N. Vigne, M. Marconi, G. Beaudoin, K. Pantzas, I. Sagnes, G. Huyet, F. Maucher, S. V. Gurevich, J. Javaloyes, A. Garnache, and M. Giudici. Temporal localized Turing patterns in mode-locked semiconductor lasers. *Optica*, 9(12):1386–1393, Dec 2022.
- [37] A. Bartolo, T. G. Seidel, N. Vigne, A. Garnache, G. Beaudoin, I. Sagnes, M. Giudici, J. Javaloyes, S. V. Gurevich, and M. Marconi. Manipulation of temporal localized structures in a vertical external-cavity surface-emitting laser with optical feedback. *Opt. Lett.*, 46(5):1109–1112, Mar 2021.
- [38] M. A. Fuentes, M. N. Kuperman, and V. M. Kenkre. Nonlocal interaction effects on pattern formation in population dynamics. *Phys. Rev. Lett.*, 91:158104, Oct 2003.
- [39] F. Maucher, T. Pohl, S. Skupin, and W. Krolikowski. Self-organization of light in optical media with competing nonlinearities. *Phys. Rev. Lett.*, 116:163902, Apr 2016.
- [40] J. Javaloyes, M. Marconi, and M. Giudici. Nonlocality induces chains of nested dissipative solitons. *Phys. Rev. Lett.*, 119:033904, Jul 2017.

Multistable Kuramoto splay states in a crystal of mode-locked laser pulses: Supplementary Material

T. G. Seidel,^{1,2} A. Bartolo,³ A. Garnache,³ M. Giudici,⁴ M. Marconi,⁴ S. V. Gurevich,¹ and J. Javaloyes²

¹*Institute for Theoretical Physics, University of Münster,
Wilhelm-Klemm-Str. 9, 48149 Münster, Germany*

²*Departament de Física and IAC³, Universitat de les Illes Balears, C/ Valldemossa km 7.5, 07122 Mallorca, Spain*

³*Institut d'Electronique et des Systèmes, CNRS UMR5214, 34000 Montpellier, France*

⁴*Université Côte d'Azur, CNRS, Institut de Physique de Nice, 06560 Valbonne, France*

I. MOTIVATION FOR THE ORDER PARAMETER

In order to measure the degree of order in a train of pulses, it is instructive to introduce an order parameter. We consider for a configuration of N pulses the first order correlation function

$$g^{(1)}(r) = \frac{\langle E^*(t) E(t+r) \rangle}{\langle |E(t)|^2 \rangle}. \quad (1)$$

This function needs to be evaluated at the position of the neighboring pulse, i.e. when N pulses are present in the cavity of size τ , we consider $g^{(1)}\left(\frac{\tau}{N}\right)$. Further, the average is defined as

$$\langle E(t) \rangle = \frac{1}{\tau} \int_0^\tau E(t) dt. \quad (2)$$

Experimentally, this makes sense as the first order correlation function can be obtained by interfering the electric field with itself after a retarded time $\frac{\tau}{N}$. Next, we consider the electric field to consist of N identical in shape and equidistant pulses. This implies that there is no shape deformation mode. The equidistance of the pulses implies that the translation mode is damped. This is the case for pulses in a relatively short cavity, where pulses are locked in position due to gain repulsion as it is the case in the experiment presented in the main part of the paper. The remaining degree of freedom is the phase φ_j of the j -th pulse such that the full field $E(t)$ reads

$$E(t) = \sum_{k=1}^N E_0\left(t - (k-1)\frac{\tau}{N}\right) e^{-i\varphi_k}, \quad (3)$$

where $E_0(t)$ is the optical field for a single pulse. Further, we define $\bar{I} \equiv \langle |E_0(t)|^2 \rangle$ as the average intensity of a single pulse. The first order correlation function then reads

$$\begin{aligned} g^{(1)}\left(\frac{\tau}{N}\right) &= \frac{\left\langle \left[\sum_{k=1}^N E_0^*\left(t - (k-1)\frac{\tau}{N}\right) e^{i\varphi_k} \right] \left[\sum_{k=1}^N E_0\left(t - k\frac{\tau}{N}\right) e^{-i\varphi_k} \right] \right\rangle}{\left\langle \left| \sum_{k=1}^N E_0\left(t - k\frac{\tau}{N}\right) e^{i\varphi_k} \right|^2 \right\rangle} \\ &= \frac{\left\langle \sum_{k=1}^N |E_0\left(t - k\frac{\tau}{N}\right)|^2 e^{i(\varphi_{k+1} - \varphi_k)} \right\rangle}{N\bar{I}} \\ &= \frac{\langle |E_0(t)|^2 \rangle}{N\bar{I}} \sum_{k=1}^N e^{i(\varphi_{k+1} - \varphi_k)} \\ &= \frac{1}{N} \sum_{k=1}^N e^{i(\varphi_{k+1} - \varphi_k)}, \end{aligned} \quad (4)$$

where we used the periodic boundaries, i.e. $E_0(t) = E_0(t - \tau)$ and considered the overlap of the pulses to be small such that we neglect all cross terms, i.e. $\left\langle \left| \sum_{k=1}^N E_0\left(t - k\frac{\tau}{N}\right) e^{i\varphi_k} \right|^2 \right\rangle = N\bar{I}$. Hence, the definition of the order parameter b in the main text corresponds to $g^{(1)}\left(\frac{\tau}{N}\right)$:

$$b \equiv g^{(1)}\left(\frac{\tau}{N}\right) = \frac{1}{N} \sum_{j=1}^N e^{i(\varphi_{j+1} - \varphi_j)}. \quad (5)$$

It makes sense to consider the limit cases of b . The modulus of b is 1, if all pulses have the same phase difference with respect to their neighbor, i.e. if $\varphi_{j+1} - \varphi_j = \beta = \text{const.} \forall j$, then

$$b = \frac{1}{N} \sum_{j=1}^N e^{i(\varphi_{j+1} - \varphi_j)} = e^{i\beta}. \quad (6)$$

In contrast, the modulus of b is 0 when the phase differences are equally spread, i.e. $\varphi_{j+1} - \varphi_j = \frac{2\pi p}{N}j$ where $p \in \mathbb{Z}$. Then

$$b = \frac{1}{N} \sum_{j=1}^N e^{i \frac{2\pi p}{N} j} = 0. \quad (7)$$

II. THE ORDER PARAMETER AS A FUNCTION OF THE NOISE AMPLITUDE AND THE NUMBER OF PULSES

In the presence of noise the order parameter b is a statistical quantity. However, we can still make predictions using the probability distribution of the phases. In the variational reciprocal case, (i.e. $\psi_{\pm} = 0$ and $A_+ = A_-$, cf. Eq. (4) of the main text) which reads

$$\begin{aligned} \dot{\varphi}_j &= \sin(\varphi_{j-1} - \varphi_j) + \sin(\varphi_{j+1} - \varphi_j) + \sigma \xi_j(t) \\ &= F_j(\varphi_1, \dots, \varphi_N) + \sigma \xi_j(t) \end{aligned} \quad (8)$$

we can define a potential that satisfies $F_j = -\frac{\partial U}{\partial \varphi_j}$

$$\begin{aligned} U &= - \int F_j(\varphi_1, \dots, \varphi_N) d\varphi_j \\ &= - \int [\sin(\varphi_{j-1} - \varphi_j) + \sin(\varphi_{j+1} - \varphi_j)] d\varphi_j \\ &= - \sum_{k=1}^N \cos(\varphi_{k-1} - \varphi_k). \end{aligned} \quad (9)$$

The Fokker–Planck equation for the probability density function (PDF) of the phase distribution $P(\varphi_1, \dots, \varphi_N, t)$ reads

$$\frac{\partial P}{\partial t} + \sum_j \frac{\partial}{\partial \varphi_j} [F_j P] = \frac{\sigma^2}{2} \sum_j \frac{\partial^2 P}{\partial \varphi_j^2}. \quad (10)$$

We solve for the steady state of the PDF, i.e. $\partial_t P = 0$. Introducing $\beta = \frac{2}{\sigma^2}$ and integrating a first time leads to

$$\sum_j F_j P = \frac{1}{\beta} \sum_j \frac{\partial P}{\partial \varphi_j} \quad (11)$$

$$\Leftrightarrow - \sum_j \frac{\partial U}{\partial \varphi_j} P = \frac{1}{\beta} \sum_j \frac{\partial P}{\partial \varphi_j}. \quad (12)$$

This equation has the solution

$$P = \mathcal{N} \exp(-\beta U), \quad (13)$$

where \mathcal{N} is a normalization constant. Its value is fixed via the integral condition

$$1 = \int P(\varphi_1, \dots, \varphi_N) d\varphi_1 \dots d\varphi_N \quad (14)$$

and therefore

$$\frac{1}{\mathcal{N}} = \int \exp\left(\beta \sum_k \cos(\varphi_{k-1} - \varphi_k)\right) d\varphi_1 \dots d\varphi_N. \quad (15)$$

To evaluate the integral we define $\theta_k = \varphi_{k-1} - \varphi_k$. However, in this notation, one variable is dependent of the other ones, i.e. we can write

$$\begin{aligned} \theta_j &= -(\varphi_1 - \varphi_N) - (\varphi_2 - \varphi_1) - (\varphi_3 - \varphi_2) - \dots - (\varphi_{j-1} - \varphi_{j-2}) - (\varphi_{j+1} - \varphi_j) - \dots - (\varphi_N - \varphi_{N-1}) \\ &= - \sum_{k \neq j} \theta_k. \end{aligned} \quad (16)$$

As a choice, we express θ_N in terms of the other phase differences. Then we have

$$\begin{aligned} \frac{1}{\mathcal{N}} &= 2\pi \int \exp \left(\beta \sum_{k=1}^{N-1} \cos \theta_k + \beta \cos \left(\sum_{k=1}^{N-1} \theta_k \right) \right) d\theta_1 \dots d\theta_{N-1} \\ &= 2\pi \int \prod_{k=1}^{N-1} \exp(\beta \cos \theta_k) \exp \left(\beta \cos \left(\sum_{k=1}^{N-1} \theta_k \right) \right) d\theta_1 \dots d\theta_{N-1} \end{aligned} \quad (17)$$

Next, we use the modified Bessel function of first kind which are defined as

$$I_n(x) = \frac{1}{\pi} \int_0^\pi \cos(n\theta) e^{x \cos \theta} d\theta. \quad (18)$$

Further, we use the following expansion in terms of the Bessel functions

$$\exp(\beta \cos \theta) = \sum_{k=-\infty}^{\infty} I_k(\beta) e^{ik\theta}. \quad (19)$$

With that we obtain

$$\begin{aligned} \frac{1}{\mathcal{N}} &= 2\pi \int \left(\sum_{n=-\infty}^{\infty} I_n(\beta) \exp(in\theta_1) \right) \dots \left(\sum_{n=-\infty}^{\infty} I_n(\beta) \exp(in\theta_{N-1}) \right) \\ &\quad \left(\sum_{n=-\infty}^{\infty} I_n(\beta) \exp \left(in \sum_{k=1}^{N-1} \theta_k \right) \right) d\theta_1 \dots d\theta_{N-1} \\ &= 2\pi \int \sum_{k_1, k_2, \dots, k_N = -\infty}^{\infty} I_{k_1}(\beta) I_{k_2}(\beta) \dots I_{k_N}(\beta) \exp(ik_1\theta_1) \exp(ik_2\theta_2) \dots \\ &\quad \exp(ik_{N-1}\theta_{N-1}) \exp \left(ik_N \sum_{l=1}^{N-1} \theta_l \right) d\theta_1 \dots d\theta_{N-1} \\ &= 2\pi \int \sum_{k_1, k_2, \dots, k_N = -\infty}^{\infty} I_{k_1}(\beta) I_{k_2}(\beta) \dots I_{k_N}(\beta) \\ &\quad \exp[i((k_1 + k_N)\theta_1 + \dots + (k_{N-1} + k_N)\theta_{N-1})] d\theta_1 \dots d\theta_{N-1}. \end{aligned} \quad (20)$$

This can also be expressed as the sum of $N - 1$ integrals. Each of these integrals has the form

$$\int_0^{2\pi} e^{i(k+l)\theta} d\theta = 2\pi \delta_{k, -l}. \quad (21)$$

Finally, we obtain

$$\begin{aligned} \frac{1}{\mathcal{N}} &= (2\pi)^N \sum_{k_1, k_2, \dots, k_N = -\infty}^{\infty} I_{k_1}(\beta) I_{k_2}(\beta) \dots I_{k_N}(\beta) \delta_{k_1, -k_N} \delta_{k_2, -k_N} \dots \delta_{k_{N-1}, -k_N} \\ &= (2\pi)^N \sum_{k_N = -\infty}^{\infty} (I_{-k_N}(\beta))^{N-1} I_{k_N}(\beta) \\ &= (2\pi)^N \sum_{k = -\infty}^{\infty} (I_k(\beta))^N \end{aligned} \quad (22)$$

and with that the PDF reads:

$$P(\varphi_1, \dots, \varphi_N) = \frac{1}{(2\pi)^N} \frac{\exp \left(\beta \sum_{k=1}^N \cos(\varphi_{k-1} - \varphi_k) \right)}{\sum_{k=-\infty}^{\infty} (I_k(\beta))^N}. \quad (23)$$

Next, we want to compute the expectation value of the order parameter. For that we can recycle the result for the normalization constant. However, we need to define the derivative of the Bessel function first:

$$\begin{aligned}\partial_\beta I_k(\beta) &= I_{k-1}(\beta) - \frac{k}{\beta} I_k(\beta) \\ &= \frac{k}{\beta} I_k(\beta) + I_{k+1}(\beta).\end{aligned}\tag{24}$$

With this we obtain

$$\begin{aligned}\langle b \rangle &= \int_0^{2\pi} \left(\frac{1}{N} \sum_k e^{i(\varphi_{k-1} - \varphi_k)} \right) P(\varphi_1, \dots, \varphi_N) d\varphi_1 \dots d\varphi_N \\ &= \frac{\mathcal{N}}{N} \int_{-\pi}^{\pi} \left(\sum_k \cos(\varphi_{k-1} - \varphi_k) \right) \exp\left(\beta \sum_k \cos(\varphi_{k-1} - \varphi_k) \right) d\varphi_1 \dots d\varphi_N \\ &= \frac{\mathcal{N}}{N} \int_{-\pi}^{\pi} \partial_\beta \exp\left(\beta \sum_k \cos(\varphi_{k-1} - \varphi_k) \right) d\varphi_1 \dots d\varphi_N \\ &= \frac{\mathcal{N}}{N} \partial_\beta \int_{-\pi}^{\pi} \exp\left(\beta \sum_k \cos(\varphi_{k-1} - \varphi_k) \right) d\varphi_1 \dots d\varphi_N \\ &= \frac{\mathcal{N}}{N} \partial_\beta \frac{1}{\mathcal{N}} \\ &= (2\pi)^N \frac{\mathcal{N}}{N} \partial_\beta \sum_{k=-\infty}^{\infty} (I_k(\beta))^N \\ &= (2\pi)^N \mathcal{N} \sum_{k=-\infty}^{\infty} (I_k(\beta))^{N-1} \partial_\beta I_k(\beta) \\ &= (2\pi)^N \mathcal{N} \sum_{k=-\infty}^{\infty} (I_k(\beta))^{N-1} \left(I_{k-1}(\beta) - \frac{k}{\beta} I_k(\beta) \right) \\ &= \frac{\sum_{k=-\infty}^{\infty} (I_k(\beta))^{N-1} \left(I_{k-1}(\beta) - \frac{k}{\beta} I_k(\beta) \right)}{\sum_{k=-\infty}^{\infty} (I_k(\beta))^N}.\end{aligned}\tag{25}$$

The last part of the sum vanishes because the sum is symmetric (from $k = -\infty$ to $k = \infty$). So we remain with

$$\langle b \rangle = \frac{\sum_{k=-\infty}^{\infty} (I_k(\beta))^{N-1} I_{k-1}(\beta)}{\sum_{k=-\infty}^{\infty} (I_k(\beta))^N}.\tag{26}$$

In the limit of $N \rightarrow \infty$, we find that the expression converges to

$$\lim_{N \rightarrow \infty} \langle b \rangle = \frac{I_1(\beta)}{I_0(\beta)}.\tag{27}$$

Further, we can look at the special case $N = 2$ where Eq. (26) converges to

$$\lim_{N \rightarrow 2} \langle b \rangle = \frac{I_1(2\beta)}{I_0(2\beta)}.\tag{28}$$

A. Approximation for low noise

An important limit case is the limit of a low noise level. For low noise we have $\sigma \rightarrow 0$ such that $\beta \rightarrow \infty$. For large arguments the modified Bessel functions of first kind can be expanded as

$$I_k(\beta) = \frac{e^\beta}{\sqrt{2\pi\beta}} \left[1 - \frac{4k^2 - 1^2}{1(8\beta)} \left(1 - \frac{4k^2 - 3^2}{2(8\beta)} \left(1 - \frac{4k^2 - 5^2}{3(8\beta)} (1 - \dots) \right) \right) \right].\tag{29}$$

We consider terms up to σ^2 , i.e. up to β^{-1} . Then we remain with

$$\begin{aligned} I_{k-1}(\beta) &= \frac{e^\beta}{\sqrt{2\pi\beta}} \left[1 - \frac{4(k-1)^2 - 1}{8\beta} + \mathcal{O}(\beta^{-2}) \right] \\ &= \frac{e^\beta}{\sqrt{2\pi\beta}} \left[1 - \frac{4k^2 - 1}{8\beta} - \frac{1 - 2k}{2\beta} + \mathcal{O}(\beta^{-2}) \right] \\ &= I_k(\beta) - \frac{e^\beta}{\sqrt{2\pi\beta}} \left(\frac{1 - 2k}{2\beta} + \mathcal{O}(\beta^{-2}) \right). \end{aligned} \quad (30)$$

As we truncate all terms $\mathcal{O}(\beta^{-2})$ we can rewrite the second term in terms of a Bessel function

$$\frac{1 - 2k}{2\beta} \frac{e^\beta}{\sqrt{2\pi\beta}} + \mathcal{O}(\beta^{-\frac{5}{2}}) = \frac{1 - 2k}{2\beta} I_k(\beta) + \mathcal{O}(\beta^{-\frac{5}{2}}) \quad (31)$$

such that

$$I_{k-1}(\beta) = \left(1 - \frac{1 - 2k}{2\beta} \right) I_k(\beta) + \mathcal{O}(\beta^{-\frac{5}{2}}). \quad (32)$$

Then we have

$$\begin{aligned} \langle b \rangle &= \frac{\sum_{k=-\infty}^{\infty} (I_k(\beta))^{N-1} \left(1 - \frac{1-2k}{2\beta} \right) I_k(\beta)}{\sum_{k=-\infty}^{\infty} (I_k(\beta))^N} \\ &= 1 - \frac{\sum_{k=-\infty}^{\infty} (I_k(\beta))^N \frac{1-2k}{2\beta}}{\sum_{k=-\infty}^{\infty} (I_k(\beta))^N} \end{aligned} \quad (33)$$

Here, the term linear in k vanishes as the sum is symmetric and we remain with

$$\begin{aligned} \langle b \rangle &= 1 - \frac{1}{2\beta} \\ &= 1 - \frac{\sigma^2}{4}. \end{aligned} \quad (34)$$

III. DISTRIBUTION OF PHASES IN THE PRESENCE OF HIGH NOISE VALUES

Figure 3 of the main text shows the time evolution of the phase differences of five pulses in the Haus master equation with added noise of amplitude $\sigma = 4 \times 10^{-4}$. The histogram in panel b) shows that the system mainly visits two phase configurations. In Fig. 1 we show the same plot for $\sigma = 10^{-3}$. Here, the distribution broadens and also other states are visited. At the same time, the inset (panel b)) shows that the average residence time for the splay states becomes shorter compared to the corresponding figure in the main text. Even though Fig. 1 exhibits a very noisy behavior for the phases, the pulse train is still perfectly regular which is demonstrated in Fig. 2. Here, an abstract over 1000 round-trips of the simulation of Fig. 1 is shown in the intensity which exhibits fluctuations of $\approx 5\%$.

IV. POSITIONS OF THE BEAT NOTES IN THE RF SPECTRUM

For an HML_N state in one of the splay phase configurations the spacing between neighboring teeth in the spectrum is N times the fundamental frequency $\nu_{FSR} = \frac{2\pi}{T}$: $\Delta\nu = N\nu_{FSR}$. Therefore, the spectrum consists of peaks located at $\nu_k = \nu_0 + k\Delta\nu$, where $k \in \mathbb{Z}$ and ν_0 is some offset around which the comb is centered. Further, in the RF spectrum the main peaks are also separated by $\Delta\nu$ and the CW beam has a frequency ν_{CW} . Hence, the beat notes in the RF spectrum for a given comb are found at $\Delta\nu_k = |\nu_{CW} - \nu_k|$. In particular, the two beat notes with the lowest frequency (cf. the sketch in the main text) are found for the value of m such that $\nu_m < \nu_{CW} < \nu_{m+1}$ and hence, $\Delta\nu_m = \nu_{CW} - \nu_0 - m\Delta\nu$ and $\Delta\nu_{m+1} = \nu_0 - \nu_{CW} + (m+1)\Delta\nu$. For simplicity, we define $\Delta\nu_0 = \Delta\nu_m + m\Delta\nu = \nu_{CW} - \nu_0$. Combining these results, we obtain

$$\Delta\nu_k = \begin{cases} +\Delta\nu_0 - k\Delta\nu & k \leq m \\ -\Delta\nu_0 + k\Delta\nu & k > m \end{cases}. \quad (35)$$

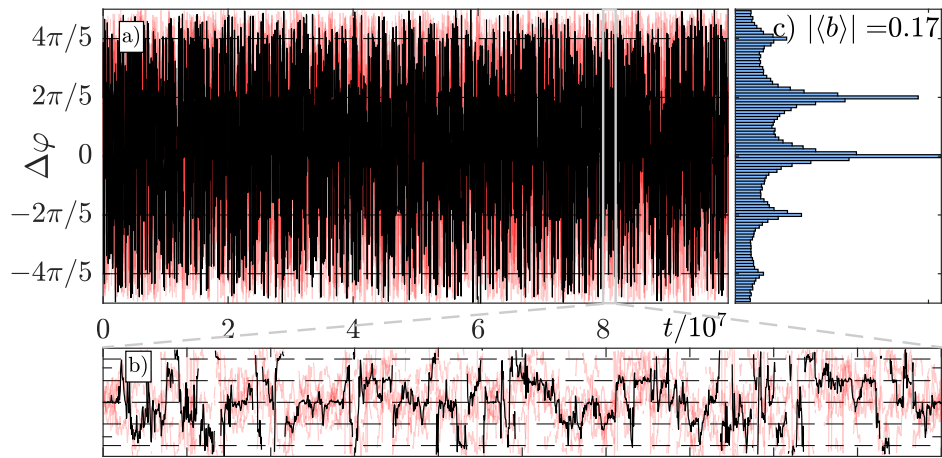


FIG. 1. Time evolution of the Haus master equation with larger noise of the amplitude $\sigma = 10^{-3}$ compared to figure 3 of the main text where $\sigma = 4 \times 10^{-4}$.

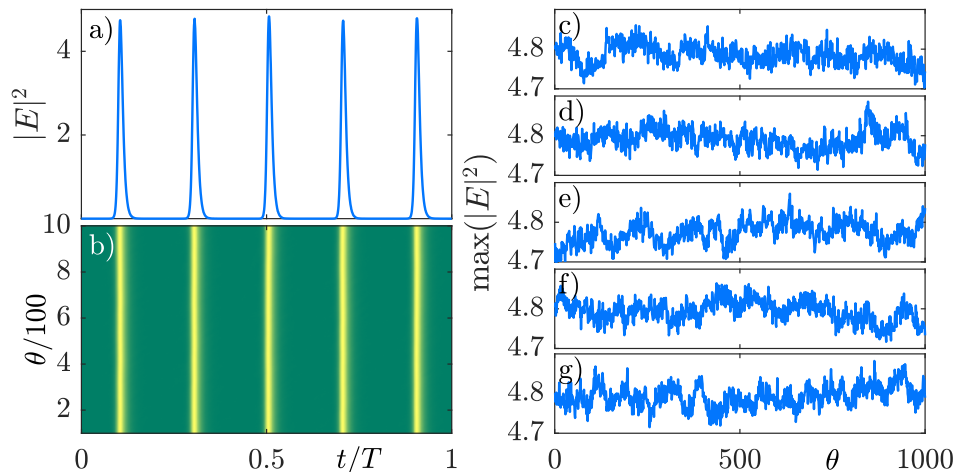


FIG. 2. Short extract of the time trace from Fig. 1. a) Profile at the last step of the simulation. b) Evolution of $|E|^2$ over 10^3 roundtrips. c)-g) Evolution of the maxima of the five pulses in a), b).

This explains why in each interval of length $\Delta\nu$ in the RF spectrum two beat notes are found corresponding to the interaction with the teeth of the comb located to the left (index m) and to the right (index $m+1$) of the CW frequency. For a visualization of the notation introduced above see Fig. 3.

A. Going from one frequency comb to the next one

In the main text, we explained that each HML_N solution has N steady states corresponding to the phase differences $\Delta\varphi_p = \frac{2\pi p}{N}$ where $p = 1, \dots, N$ which correspond to a shift of the frequency comb by $p\nu_{FSR} = p\frac{2\pi}{\tau}$. Hence, ν_0 is shifted by $p\nu_{FSR}$. Therefore, we introduce the index p in the previous notation such that $\Delta\nu_k^{(p)} = |\nu_{CW} - \nu_k^{(p)}|$ where $\nu_k^{(p)} = \nu_0 - p\nu_{FSR} + k\Delta\nu$. Hence, in general, there are $2N$ possible positions for the beat notes in each interval of size $\Delta\nu$ in the RF spectrum (cf. Fig. 4).

Next, we want to make conclusions on the phase relation of the pulses in two different RF spectra p and q based on the respective locations of the beat notes. We consider the beat notes $\Delta\nu_{m,+}^{(p)}$ and $\Delta\nu_{m,+}^{(q)}$. As expected, the distance

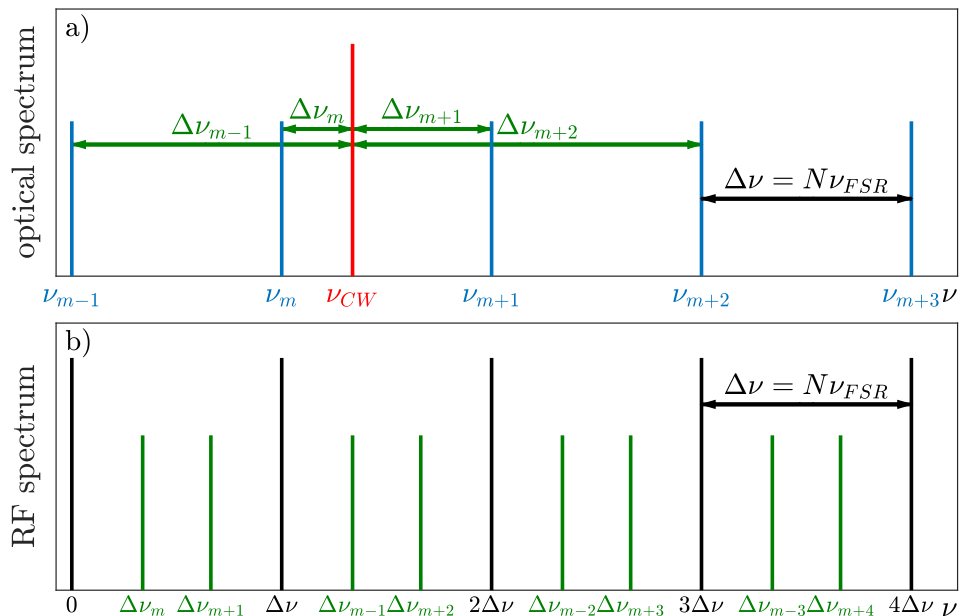


FIG. 3. a) The optical spectrum of HML_N state in a splay phase configuration where the peaks of the comb are separated by $N\nu_{FSR}$. We use a CW beam (red) to create beat notes (green). b) The RF spectrum with the beat notes shown in a).

between these quantities gives a multiple of $\Delta\nu$

$$\begin{aligned}\Delta\nu_m^{(p)} - \Delta\nu_m^{(q)} &= \Delta\nu_0^{(p)} - m\Delta\nu - \Delta\nu_0^{(q)} + m\Delta\nu \\ &= (p - q)\nu_{FSR}\end{aligned}\quad (36)$$

In the same way, we can also relate the left and the right beat notes of two different spectra p and q

$$\begin{aligned}\Delta\nu_m^{(p)} + \Delta\nu_{m+1}^{(q)} &= \Delta\nu_0^{(p)} - m\Delta\nu - \Delta\nu_0^{(q)} + (m + 1)\Delta\nu \\ &= (p - q)\nu_{FSR} + \Delta\nu.\end{aligned}\quad (37)$$

V. EXPERIMENTAL SETUP

The experimental setup is shown in Fig. 5. It consists in a Vertical External-Cavity Surface-Emitting Laser (VECSEL) delimited by an optically pumped InGaAs gain mirror emitting at 1060 nm and by a Semiconductor saturable Absorber Mirror (SESAM). The layout of the VECSEL cavity is similar to the one described in [1] and it is operated in the regime of temporal localized structures where multiple mode-locked pulses circulate in the resonator and each pulse can be individually addressed by shining short pump pulses inside the cavity [1]. For the heterodyne measurement, we use a tunable Littman-Metcalf diode laser system from Sacher with a linewidth smaller than 100 kHz. The resolution of the spectral detection is set by the RF power analyzer and amounts to 300 kHz.

VI. EXPERIMENTAL RESULTS WITH A SPLAY STATE OF 6 PULSES

Lastly, Fig. 6 shows that coherent splayed state and incoherent pulse trains can be obtained for a larger number of pulses in the external cavity. Similarly to the 4 pulses case, Fig. 6 shows a splayed state of 6 pulses (panel a) and an incoherent phase state (panel b).

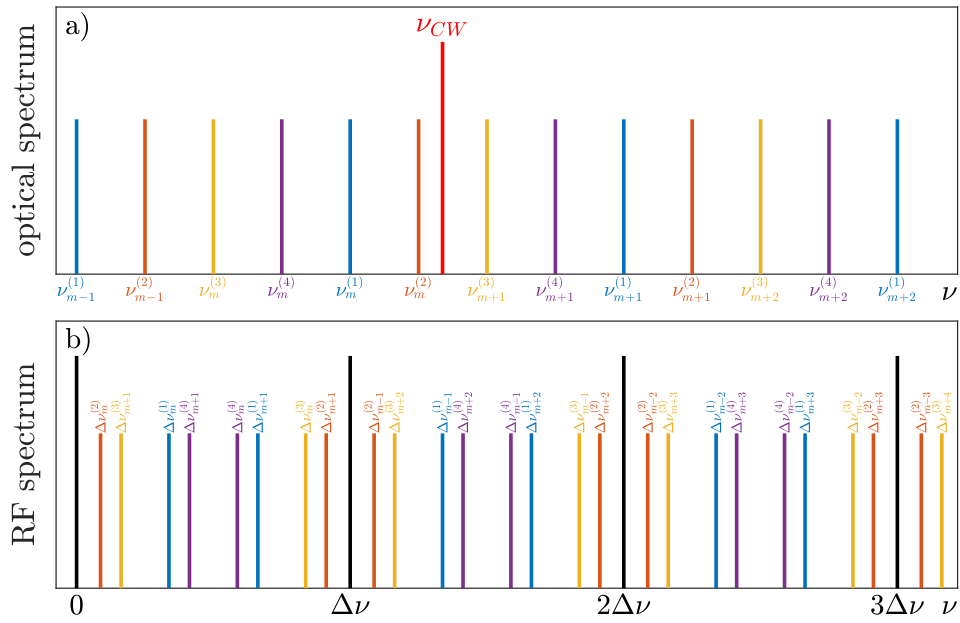


FIG. 4. a) The optical spectrum of HML₄ state in a non-splay phase configuration. Here, the comb is a superposition of the four sub-combs shown in green, orange, yellow and purple. The separation of two e.g. blue peaks is $\Delta\nu = 4\nu_{FSR}$ while neighboring peaks (e.g. blue and orange) are separated by ν_{FSR} . We use a CW beam (red) to create beat notes. b) The RF spectrum with the beat notes. In each interval of size $\Delta\nu$, we find 8 beat notes.

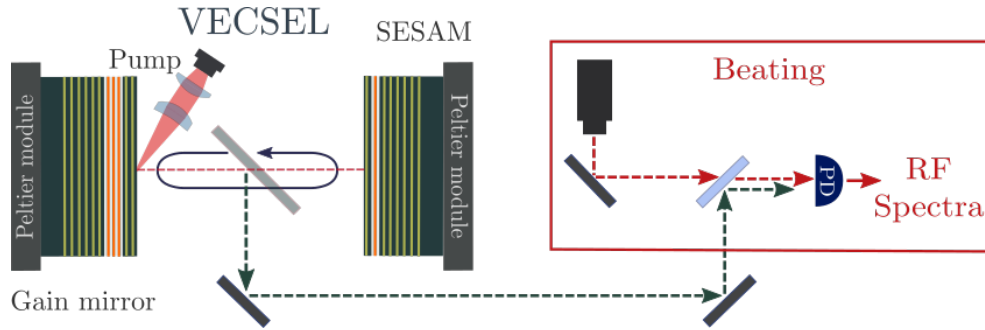


FIG. 5. Experimental setup of the mode-locked VECSEL and detection. PEM: Piezo-Electric Mirror. PD: Photodiode. The heterodyne beating is realized between a tunable laser source (red arrow) and the VECSEL output (green arrow).

VII. REFERENCES

- [1] A. Bartolo, N. Vigne, M. Marconi, G. Beaudoin, K. Pantzas, I. Sagnes, G. Huyet, F. Maucher, SV Gurevich, J. Javaloyes, A. Garnache and M. Giudici, Temporal localized Turing patterns in mode-locked semiconductor lasers, *Optica* 9, 1386-1393 (2022).

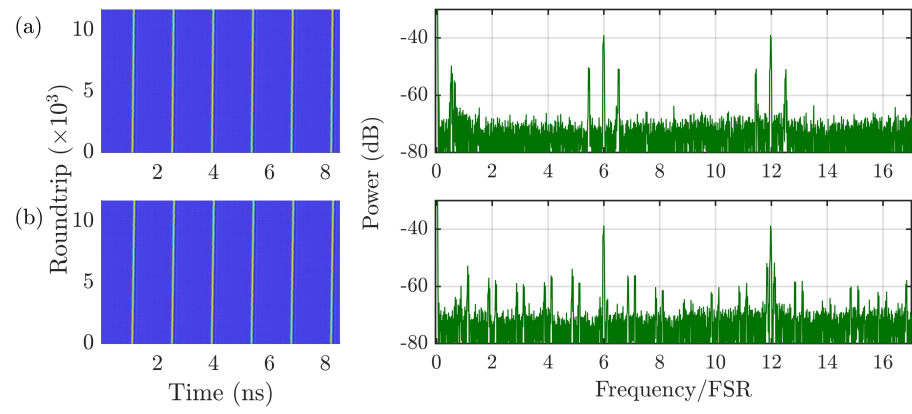


FIG. 6. Analysis of the played states of 6 pulses emitted by the mode-locked VECSEL. Left column: spatio-temporal maps of the laser intensity. Right column: RF spectrum of the heterodyne beating signal. a) Coherent splayed states. b) Incoherent state characterized by the average spectral emission composed by spectral lines separated by 1 FSR.